Check for updates

Polyoxometalate nanocluster-infused triple IPN hydrogels for excellent microplastic removal from contaminated water: detection, photodegradation, and upcycling†

Soumi Dutta, [ID] * Ashok Misra and Suryasarathi Bose [ID] *

Microplastic (MP) pollution pervades global ecosystems, originating from improper plastic disposal and fragmentation due to factors like hydrolysis and biodegradation. These minute particles, less than 5 mm in size, have become omnipresent, impacting terrestrial, freshwater, and marine environments worldwide. Their ubiquity poses severe threats to marine life by causing physical harm and potentially transferring toxins through the food chain. Addressing this environmental crisis necessitates a sustainable strategy. Our proposed solution involves a highly efficient copper substitute polyoxometalate (Cu-POM) nanocluster infused triple interpenetrating polymer network (IPN) hydrogel, comprising chitosan (CS), polyvinyl alcohol (PVA), and polyaniline (PANI) (referred to as pGel@IPN) for mitigating MP contamination from water. This 3D IPN architecture, incorporating nanoclusters, also enhances the hydrogel's photodegradation capabilities. Our scalable approach offers a sustainable strategy to combat MPs in water bodies, as demostrated by the adsorption behaviors on the hydrogel matrix under varying conditions, simulating real-world scenarios. Evaluations of physicochemical properties, mechanical strength, and thermal behavior underscore the hydrogel's robustness and stability. Detecting minute MP particles remains challenging, prompting us to label MPs with Nile red for fluorescence microscopic analysis of their concentration and adsorption on the hydrogel. The catalytic properties of POM within the hydrogel facilitate UV-induced MP degradation, highlighting a sustainable solution. Our detailed kinetics and isotherm studies revealed pseudo-first-order and Langmuir models as fitting descriptors for MP adsorption, exhibiting a high maximum adsorption capacity (Q_m). Notably, pGel@IPN achieved ~95% and ~93% removal efficiencies for polyvinyl chloride (PVC) and polypropylene (PP) MPs at pH ~ 6.5, respectively, also demonstrating reusability for up to 5 cycles. Post-end-of-life, the spent adsorbent was efficiently upcycled into carbon nanomaterials, effectively removing the heavy metal Cr(VI), exemplifying circular economy principles. Our prepared hydrogel emerges as a potent solution for MP removal from water, promising effective mitigation of the emerging pollutants of MPs while ensuring sustainable environmental practices.

1. Introduction

Microplastics (MPs) represent a pressing environmental threat, comprising minute plastic particles, often measuring less than 5 mm, and even smaller nanoplastics, causing widespread pollution across terrestrial, freshwater, and marine ecosystems.[1–3] The proliferation of plastic usage, compounded by improper waste management practices, results in the generation and accumulation of MPs through processes like hydrolysis, photodegradation, and mechanical abrasion. These pollutants pervade various environments, from remote polar regions to deep ocean trenches, posing grave risks to marine life. Ingested by a spectrum of organisms, MPs traverse the food chain, potentially transferring toxins and persisting organic pollutants, amplifying their toxicity.[4,5] This literature review indicates that numerous studies have explored the field of MP remediation.[6–9] Our research addresses gaps in sustainable MPs remediation by employing a circular economy approach, encompassing adsorption, degradation, reusability, and upcycling. We have synthesized an innovative nanocluster-infused triple interpenetrating polymer network (IPN) hydrogel for the efficient removal of MPs from water. Hydrogels, with tunable properties and unique 3D structures, show promise in sustainable water purification.[10,11]

Department of Materials Engineering, Indian Institute of Science, Bengaluru 560012, India. E-mail: soumidutta.ce@gmail.com, sbose@iisc.ac.in

Herein, IPN hydrogels comprising chitosan (CS), polyvinyl alcohol (PVA), and polyaniline (PANI) are used as a potent solution for removing MPs from water, leveraging their distinctive structural and functional attributes. An IPN is formed by combining two or more polymer networks, with at least one polymer synthesized or crosslinked in the presence of others, resulting in an interconnected network structure.[12–14] The focus here is on a unique semi-IPN structure composed of PVS, CS, and the sequential polymerization of the PANI polymer from the aniline monomer within the existing networks.[12,15] The innovative triple IPN architecture allows for customizable hydrogel formation, offering a tunable pore size and mechanical flexibility, enhancing efficient MP adsorption and capturing with its three-dimensional configuration.[12,13] Besides, the established reusability and compatibility with diverse water remediation techniques make these hydrogels versatile and sustainable options for combating the escalating issue ofMPs pollution in aquatic ecosystems.[7,11,16]

Our developed hydrogel, mainly a blend of PVA and CS, presents a compelling solution for various environmental applications,[17,18] here particularly in the removal of MP contaminants from water. PVA contributes to the hydrogel's mechanical strength, flexibility, and water retention capacity, attributed to its high hydrophilicity and biocompatibility.[17,19] Additionally, PVA provides abundant hydroxyl functional groups for cross-linking and hydrogel formation.[20] Conversely, CS, derived from chitin, is another excellent candidate for

Dr. Soumi Dutta is currently a postdoctoral research fellow in the Materials Engineering Department at the Indian Institute of Science (IISc), Bangalore, supported by the IoE IISc post-doctoral fellowship. She earned her Ph.D. in 2022 from the School of Water Resources at the Indian Institute of Technology Kharagpur (IIT Kharagpur). Prior to that, she obtained her Master's in Engineering (M.E.) degree from Jadavpur University in 2016 and her Bachelor's (B.E.) degree in Civil Engineering from the University of Burdwan in 2013. Dr. Dutta's research focuses on the synthesis of cutting-edge nanomaterials and IPN-based membranes and hydrogels for environmental remediation, particularly in water treatment. She has contributed to this field through publishing several research articles and active participation in international conferences with fellowship support. Her dedication extends to protecting natural resources, particularly water, from emerging contaminants using advanced treatment solutions. Beyond her academic pursuits, she enjoys classical dancing, traveling, drawing, crafting, gardening, and exploring diverse cuisines.

Soumi Dutta

hydrogel formation due to its biocompatibility, biodegradability, and antimicrobial properties.[21,22] It exhibits remarkable adsorption properties, forming complexes with MPs through electrostatic interactions. Additionally, the hydroxyl groups of PVA and the amino groups of CS engage in hydrogen bonding, creating a strong intermolecular network.[23] This interaction augments the hydrogel's mechanical strength and swelling behavior. The resulting synergy imparts heightened adsorption efficiency, improved water retention, biodegradability, and reduced toxicity, positioning the hydrogel as an ideal choice for eco-friendly MP removal in aquatic environments. Furthermore, the introduction of PANI into these hydrogel matrices increases the polymeric entanglement, pore tuning properties, and mechanical robustness and improves adsorption capabilities through its unique conductivity, stability, and increased surface area.[24–27] Furthermore, the presence of functional groups, particularly amino groups from chitosan and PANI, within the IPN hydrogel, played a crucial role in attracting and facilitating the adsorption of negatively charged MP particles. The synergistic benefits of all three polymers make it a multifunctional IPN hydrogel that offers a sustainable solution by successfully trapping MP by polymeric entanglement and adsorption *via* functional groups, demonstrating its remediation potential.

Polyoxometalates (POMs) are complexes of transition metal–oxygen clusters and are renowned for their high electronegativity, oxo-enriched surface, programmable shape and size, redox potential, and tunable acid–base properties. Specifically, Keggin-type POMs are widely utilized in photocatalytic degradation, offering significant promise for addressing environmental challenges related to the removal of organic pollutants. The Keggin structure is characterized by a central heteroatom (typically a transition metal) surrounded by a cage of oxygen atoms, represented by the general formula $H_3PM_{12}O_{40}$.[28] These clusters feature a central PO_4 tetrahedron surrounded by 12 MO_6 octahedra (M = Mo, W), organized into four groups of three edge-sharing M_3O_{13}. Each group shares an oxygen atom with the central PO_4 tetrahedron. However, substituting Mo^{6+} ions with transition metals (TMs) such as Cu^{2+} introduces an excess negative charge that needs compensation. In our study, we synthesized copper-substituted polyoxometalate (Cu-POM) using a one-step hydrothermal process.[28–31] However, the suitable band gap, stability, and simple fabrication of POMs contribute to their appeal in addressing environmental challenges, supporting our incorporation of these unique nanoclusters for enhancing microplastic photodegradation in water.[32–34]

In this study, we have engineered a sustainable triple interpenetrating polymer network (IPN) hydrogel, designated as pGel@IPN, incorporated with polyoxometalate (POM) nanoclusters, to effectively address the removal of MPs from water. Our investigation specifically targeted two model MPs, polyvinyl chloride (PVC) and polypropylene (PP). Systematic analyses were conducted to evaluate MPs' adsorption under varying conditions, including solution pH, hydrogel dosage, and contact time, emulating real-world scenarios. Thorough

investigations encompassing adsorption isotherms, kinetics, and thermodynamics provided insights into the intricate mechanisms governing MPs' adsorption. The comprehensive study incorporates pGel@IPN hydrogel synthesis for MP adsorption, advanced detection methodologies, material characterization, photodegradation of MPs, and an innovative upcycling approach, culminating in the establishment of a closed-loop circular economy. This holistic approach contributes significantly to sustainable and eco-friendly microplastic remediation.

2. Experimental section

2.1. Materials

Chitosan (CS) was obtained from HiMedia Laboratories, LLC, and lab reagent (LR) grade polyvinyl alcohol (PVA) was procured from IndiaMart. Copper sulfate pentahydrate ($CuSO_4 \cdot 5H_2O$), molybdic acid ($MoO_3 \cdot H_2O$), phosphoric acid (H_3PO_4), ethylenediamine, and terephthalic acid (H_2BDC) were acquired from Sigma Aldrich. Hydrochloric acid (HCl, 35–38%) was sourced from SD Fine Chemicals Ltd in Mumbai, India. Aniline (PANI, 99.5%) was obtained from Sectrochem Pvt. Ltd, and reagent-grade ammonium persulfate (APS, 98%) was supplied by Sigma Aldrich. All these materials were used without any additional processing or purification.

2.2. Preparation of Kegging-type copper-polyoxometalate nanoclusters

The synthesis of the Keggin-type copper substitute polyoxometalate (Cu-POM) employed a straightforward one-step hydrothermal process, adapted and refined from earlier literature,[28–31] with minor modifications. Initially, 1.5 g of $CuSO_4 \cdot 5H_2O$ was dissolved in 180 ml of deionized water within a glass container. Following this, a mixture of 4.5 g of $MoO_3 \cdot H_2O$, 1.4 ml of ethylene diamine (en), and 2.5 ml of H_3PO_4 was added concurrently to the solution. The components were thoroughly blended using a magnetic stirrer at room temperature (25 ± 3 °C). Subsequently, the resulting mixture was transferred to a Teflon-lined hydrothermal autoclave and placed in an oven set at 200 °C for 72 hours. Finally, the obtained precipitate was centrifuged and washed multiple times with deionized water and subjected to oven-drying to yield the Cu-POM nanocluster powder.

2.3. Preparation and structural description of the POM-infused PVA-chitosan-PANI@IPN hydrogel

In the synthesis of the Cu-POM-infused triple interpenetrating polymer network (IPN) hydrogel, 2 g of polyvinyl alcohol (PVA) was stirred in 50 ml of distilled water at 70 °C for 4 h. Simultaneously, 2 g of chitosan (CS) in a 2% v/v aqueous acetic acid solution was agitated at 60 °C for 4 h. Additionally, 1 g of Cu-POM was dispersed in 10 ml of deionized water through probe-sonication. The solutions of PVA, CS, and POM were then mixed, and 1 ml of aniline monomer doped with 1 M HCl was added. After blending the solution for 6 hours to

ensure homogeneity, aniline underwent sequential interpenetrating polymerization upon the addition of an equimolar ammonium persulfate (APS) aqueous solution dropwise. The reaction occurred in an ice bath for 12 hours, leading to the formation of polyaniline (PANI). This contributed to the development of the triple (PVA-CS-PANI) IPN hydrogel, denoted as Gel@IPN. To enhance mechanical stability, a 1% v/v aqueous glutaraldehyde solution was added dropwise for cross-linking the IPN hydrogel matrix. Finally, the blend was poured into a Petri dish, and dried at room temperature, to form the POM-infused triple IPN hydrogel (pGel@IPN). Subsequently, the hydrogel was washed thoroughly to remove residual chemicals by immersing it in DI water for a week, with daily water changes. Fig. 1 schematically illustrates the synthesis process of the hydrogel matrix, offering insights into potential chemical interactions among its components.

The created hydrogel is classified as a semi-IPN hydrogel because during the hydrogel synthesis process, in the presence of PVA and CS polymer networks, the PANI network is polymerized from its monomer (aniline) in the presence of an ammonium persulphate initiator.[12,15] However, the polymeric network of semi-IPN hydrogel forms through crosslinking, where the amine group of chitosan interacts with the aldehyde group of glutaraldehyde (GA), creating stable imine bonds.[35–37] This reaction generates imine groups *via* nucleophilic addition of chitosan to GA's aldehyde group, resulting in hemiaminal bridges (–C(OH)(NHR)–) and a Schiff base reaction.[38,39] Additionally, the hydroxyl group of PVA crosslinks with aldehyde groups of GA *via* acetal bonding,[38,39] while forming hydrogen bonds with chitosan[17,18] (denoted by red dotted lines in Fig. 1b). This crosslinking continues until all chitosan's amino groups and PVA's hydroxyl groups interact with aldehyde groups of GA, creating a stable hydrogel network.[40] The PANI network formation within the hydrogel, leading to its transformation from transparent to dark green color, occurs through the interpenetration of the PANI polymer chain.[41] Additionally, POM nanoclusters are physically integrated into the IPN hydrogel matrix *in situ* and can be attached to it through multiple approaches. *In situ* polymerization enables the creation of POM/polymer hybrid hydrogel materials.[42] POMs disperse uniformly in polar monomers, forming hybrids through *in situ* polymerization. In the literature by Lan *et al.*,[42] a polypyrrole film with POMs is produced during pyrrole polymerization. Similarly in our synthesis, aniline and POM form a homogeneous solution, undergoing oxidative polymerization with ammonium persulphate to yield POM-containing PANI within the IPN hydrogel matrix. An additional approach involves anchoring POMs into polymer matrices through electrostatic interactions. Electrostatic interactions involve positively charged PANI electrostatically tagging with the negatively charged POM cluster, illustrating POM attachment to the IPN hydrogel matrix as depicted in Fig. 1. A similar mechanism has been reported in the literature,[43] where *in situ* polymerization of aniline links negatively charged layers of POM-stabilized platinum nanoparticles with positively charged polyaniline layers, resulting in stable hybrid

Fig. 1 Schematic representation of the synthesis of the POM-infused triple network IPN hydrogel; (a) a photograph of the hydrogel held in the hand, demonstrating its flexibility and (b) a schematic illustration of the pGel@IPN hydrogel internal architecture and the plausible chemical interaction to form the IPN hydrogel.

films. Moreover, the tunable functional groups in POM derivatives show the potential for covalent anchoring into diverse polymer matrices, through copolymerization with various monomers, presenting an alternative viable route.[44] All the plausible mechanisms of pGel@IPN hydrogel formation are depicted in Fig. 1.

2.4. Preparation of microplastic pollutant

In this study, two model MPs, PVC and PP, were used. The PVC-MP powder was obtained from a local market and subjected to a thorough washing process with deionized (DI) water. In contrast, the PP-MP was produced by grinding waste food containers, and then cleaned by immersion in a 1 M HCl solution at 60 °C for 6 h. Afterward, it was rinsed with DI water. Both types of MPs were sieved through a 150 μm mesh to ensure a uniform particle size. Subsequently, the sieved particles were meticulously washed again and dried for further analysis.

2.5. Fluorescence staining for the detection of microplastic particles

The detection and quantification of MPs is a challenging task. In this study, we tackle this challenge by utilizing the fluorescence staining technique on MPs, followed by their detection through fluorescence spectroscopy. In this process, Nile Red, a fluorescent dye (Sisco Research Laboratories Pvt. Ltd, India) ($C_{20}H_{18}N_2O_2$, M.W. 318.37), is employed to stain the MP particles. The staining solution is prepared by dissolving Nile Red in methanol (chosen for its compatibility with plastics) at a concentration of 1 μg L^{-1}.[3] Subsequently, the MPs are immersed in this staining solution for 8 h while being subjected to a controlled temperature cycle (ranging from 0 °C to 70 °C) to enhance the fluorescence efficacy and prevent dye leaching.[3] Afterward, the staining solution is filtered to collect the fluorescence-stained MPs, which typically appear light purple in color (Fig. 2). Finally, these MP particles are washed with deionized water to eliminate any unabsorbed dye and
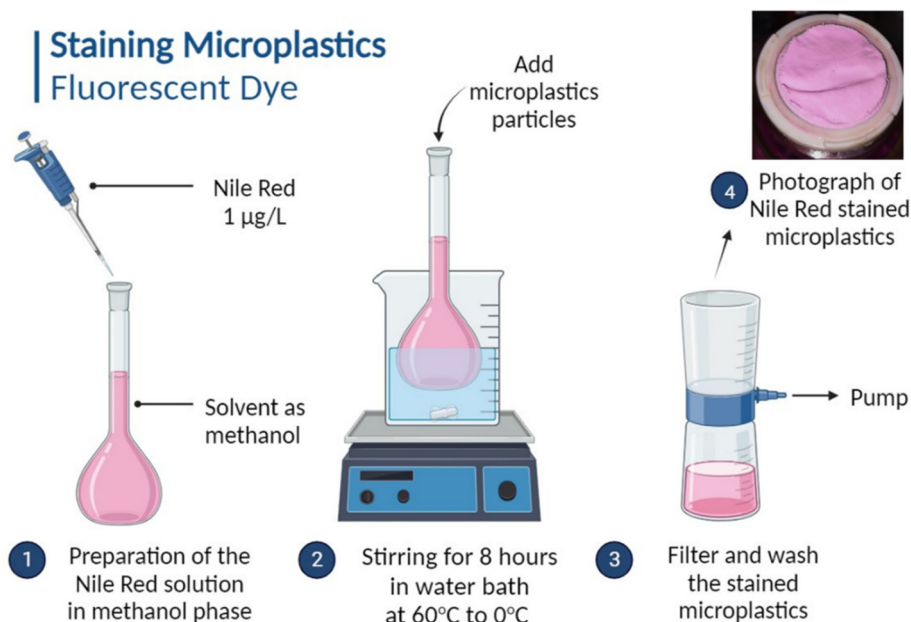
Fig. 2 Schematic illustration of the MP staining process using the fluorescent dye Nile red for MP detection following adsorption in hydrogel matrices.

then dried at 60 °C in a vacuum oven for further analysis and application. Fig. S4a† exhibits the fluorescent Nile red dye-tagged PVC-MPs with varying concentrations and their corresponding wavelengths. Additionally, the graph (Fig. S4b†) showcases the calibration curve fitting for the detection of MPs, providing an analytical framework for quantifying MP concentrations based on the fluorescence intensity.

2.6. Material characterization

Various characterization techniques were employed to assess the morphology and interactions of pGel@IPN with MPs, precisely polypropylene (PP) and polyvinyl chloride (PVC). Scanning electron microscopy (SEM) with energy-dispersive X-ray (EDX) analysis was used to examine the surface morphology of both the hydrogel and MPs. Fourier transform infrared spectroscopy (FTIR) enabled the identification of chemical components within pGel@IPN and the MP pollutants. X-ray photoelectron spectroscopy (XPS) was employed to investigate the surface chemistry and the electronic state of polyoxometalate (POM) within the hydrogel matrix. X-ray diffraction (XRD) analysis provided insights into the crystal structure of both the hydrogel and MPs. Thermogravimetric analysis (TGA) assessed the thermal stability of the interpenetrating polymer network (IPN) hydrogel. Contact angle measurements using water as the solvent evaluated the hydrogel's hydrophilicity (details described in ESI S1†). Mechanical tensile properties (stress *vs.* strain) of the hydrogel were assessed using a Universal Testing Machine (UTM) at a 1 mm min^{-1} tensile rate, applying a 25 N cell load to dumbbell-shaped samples (as shown in inset Fig. 5f). Zeta potential analysis determined the electrical surface charge characteristics of the hydrogel and MPs, assessing potential electrostatic interactions. Fluorescence confocal microscopy aided in the detection of fluorescently tagged MPs adsorbed within the pGel@IPN hydrogel. This technique was also used to measure the MP concentration in water, and a calibration curve was established based on these measurements. These comprehensive characterization methods provide essential information on the structure, composition, and behavior of the hydrogel and its interaction with MPs, aiding in the verification of MP adsorption by pGel@IPN.

2.7. Swelling experiments of the IPN hydrogels

The swelling properties of the polymer-based hydrogels, specifically pGel@IPN with varying crosslinking concentrations (GA: 0%, 1%, 3%, and 5% v/v), were investigated by immersing the samples in deionized water at room temperature (25 ± 3 °C). Pre-dried hydrogels were initially weighed (W_0) before immersion. After different time intervals, the samples were carefully taken out from water, excess water was wiped off with filter paper, and their weight was measured to determine the wet weight (W_s) over the immersion period. The swelling ratio (S) is calculated using eqn (1):[45]

$$S(\%) = \frac{W_s - W_0}{W_0} \times 100 \tag{1}$$

Each water absorption experiment was replicated three times, and the average value was considered to validate the results.

2.8. Microplastics adsorption experiment by the hydrogel

Batch adsorption experiments were carried out in 100 mL Borosil glass bottles with varying initial concentrations of

aqueous MP solutions and hydrogel doses (0.5 g L^{-1} to 5 g L^{-1}) at room temperature in a shaker incubator at 25 °C. In the experiment, a single variable was varied, and other conditions were maintained constant. From literature review, it is observed that the concentrations, types, and shapes of MPs can vary significantly depending on environmental conditions. MPs are frequently present in freshwater and drinking water, and their concentrations spanned ten orders of magnitude (1 × 10^{-2} to 108 numbers per m^3) across individual samples and water types.[1] Consequently, in our study, we are trying to mimic all possible conditions of actual MP contaminated water by taking a wide range of MP concentrations under various conditions. Adsorption isotherm studies encompassed MP concentrations ranging from 0.25 mg L^{-1} to 200 mg L^{-1}, with a fixed 1 g L^{-1} hydrogel dose. Specific concentrations of the fluorescence-tagged MPs were prepared by diluting a 200 mg L^{-1} MP stock solution in DI water. The effect of pH on MP removal was explored over a range from pH 2 to 12, keeping other factors constant. Kinetics studies were conducted at different intervals (10–1440 min) to analyze MPs uptake by the 1 g L^{-1} hydrogel. A thermostatic shaker was used to rotate all batches of experiments at 150 ± 10 rpm. A fluorescence spectrophotometer (532 nm laser) assessed residual MPs after separating the hydrogel from water. A calibration curve was derived from known MP concentrations. The % removal of MPs was calculated using eqn (2):

$$\% \text{ Removal of MPs} = \frac{(C_0 - C_t)}{C_0} \times 100 \quad (2)$$

The initial MP concentration is denoted as C_0 (mg L^{-1}), and C_t (mg L^{-1}) represents the MP concentration at a specific time "t". Eqn (3) is used to calculate the adsorption capacity of the hydrogel at time "t".

$$q_t = \frac{(C_0 - C_t)V}{m} \quad (3)$$

where "m" (g) signifies the mass of the hydrogel and "V" (L) stands for the volume of the MP aqueous solution. The photo-degradation of MPs was carried out in a controlled environment at 25 °C using a UV reactor illuminated with a 420 nm UV lamp. This process involved a specific concentration of MPs in deionized (DI) water alongside 1 g of hydrogel under continuous magnetic stirring for a duration of 10 hours.

2.9. Adsorption kinetics and isotherms

The rate of MP adsorption onto the hydrogel matrix is governed by diverse physicochemical interactions at the interfaces of solid and liquid, which can be elucidated through adsorption kinetic models.[27] In this study, data from the time study experiment for MP adsorption are subjected to fitting with three kinetic models: pseudo-first-order kinetics, pseudo-second-order kinetics, and the Weber–Morris equation intra-particle diffusion models, represented by eqn (4), (5), and (6), respectively:[26]

$$q_t = q_e(1 - e^{-k_1 t}) \quad (4)$$

$$q_t = \frac{(k_2 q_e^2 t)}{(1 + k_2 q_e t)} \quad (5)$$

$$q_t = k_d t^{0.5} + C \quad (6)$$

Here, q_e (mg g^{-1}) signifies the adsorption capacity of MPs at equilibrium. The parameters k_1 (min^{-1}) and k_2 (g mg^{-1} min^{-1}) denote the rate constants for pseudo-first-order and pseudo-second-order kinetics. The k_d (mg g^{-1} min$^{-0.5}$) and C values represent the rate constant for intraparticle diffusion and the thickness of the boundary layer, respectively. The adsorption equilibrium phenomenon at the interface of the adsorbent (hydrogel) and adsorbate (MPs) is explained through adsorption isotherm studies, providing insights into the adsorption mechanism. Experimental data, with varying initial MP concentrations, are fitted to two theoretical isotherm models, namely Langmuir and Freundlich isotherms. The Langmuir isotherm model, suggested monolayer adsorption, is defined as follows:[27]

$$q_e = \frac{Q_m b C_e}{1 + b C_e} \quad (7)$$

The Freundlich isotherm model accommodates multilayer adsorption and is described by eqn (8) that reflects the non-restricted, heterogeneous nature of the adsorption process:

$$q_e = K_f C_e^{\frac{1}{n}} \quad (8)$$

where, K_f and n are the Freundlich constant corresponding to the adsorption capacity [(mg g^{-1}) (L mg^{-1})$^{1/n}$] and intensity of adsorption, respectively. These models represented the MP adsorption process onto pGel@IPNs.

3. Results and discussion

3.1. Materials characterization study

Hierarchical morphology of the IPN hydrogel and MPs. The scanning electron microscopy (SEM) analysis was conducted to investigate the surface morphology of the IPN hydrogel before and after infusion of POM as depicted in Fig. 3(a and b), respectively. Gel@IPN crosslinked with glutaraldehyde (GA) showcased a diverse structural morphology of the hydrogel, exhibiting both porous and denser regions (Fig. 3a). Upon POM infusion into the Gel@IPN hydrogel architecture, distinct POM nanoclusters became visibly embedded within the pGel@IPN hydrogel matrix, as depicted in Fig. 3b. The hydrothermal synthesis of Cu-POM nanoclusters incorporated into the hydrogel demonstrated a significant enhancement in the hydrogel's charge carrying capacity, coupled with reinforced mechanical strength due to its crosslinking IPN with GA. The inclusion of Cu-POM into Gel@IPN was further confirmed by elemental analysis using energy-dispersive X-ray spectroscopy (EDX) mapping of pGel@IPN, showcasing a uniform distribution of C, N, O, Mo, P, and Cu (ESI Fig. S1(a–h)†). Furthermore, SEM analysis of PVC-MPs (Fig. 3c) illustrated a consistent spherical morphology, with an average diameter of
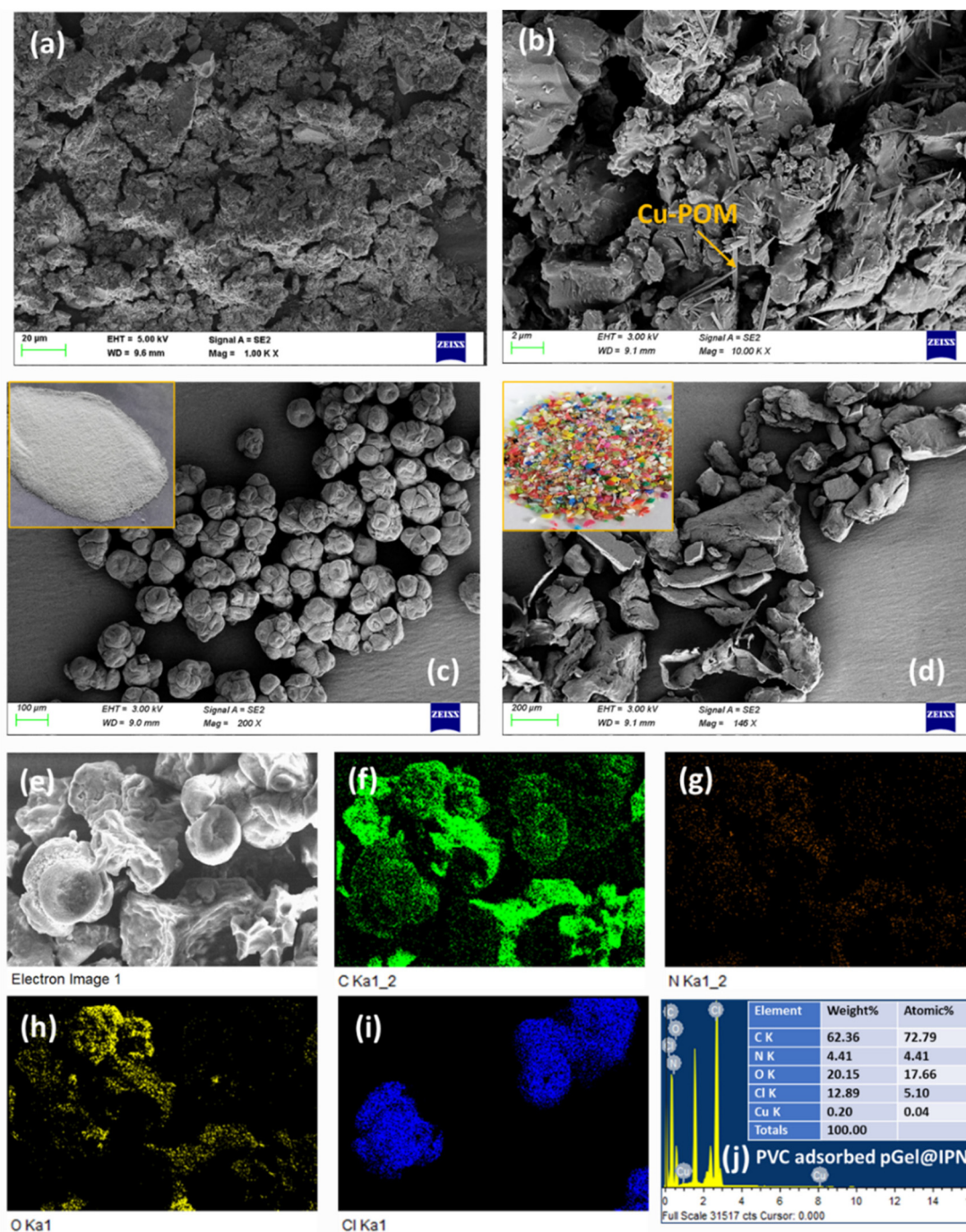
Fig. 3 Scanning electron microscopy (SEM) images of (a) Gel@IPN, (b) pGel@IPN, (c) commercial PVC-MPs (inset: a digital photograph), and (d) laboratory-synthesized PP-MPs (inset: a digital photograph), (e) PVC-MPs adsorbed pGel@IPN hydrogel and (f–i) energy-dispersive X-ray (EDX) elemental mapping of elements C, N, O, and Cl, respectively, of the PVC-MPs adsorbed pGel@IPN matrix, and (j) the EDX spectrum and composition of PVC-MPs adsorbed pGel@IPN hydrogel.

approximately 100 μm. The inset in Fig. 3c presented the images of pristine PVC-MP powder obtained from industrially synthesized sources, revealing a clean surface devoid of additives or signs of environmental aging effects. In contrast, Fig. 3d depicts the SEM images of PP-MPs, displaying irregular shapes. The observed morphology was in accordance with the

lab-scaled preparation process, as evidenced by the inset in Fig. 3d, presenting a photographic representation of PP-MPs. Further insights into the elemental compositions of both PVC and PP-MPs are provided in the ESI (Fig. S1(i and j)†). SEM imaging conducted on the spent hydrogels following the adsorption of PVC-MPs revealed the clear capture of MPs

within the structural framework of the pGel@IPN hydrogel, as displayed in Fig. 3e. Elemental mapping using EDX distinctly illustrates the presence of PVC-MPs captured on the hydrogel matrix, depicted as evidence in Fig. 3(f–i). Fig. 3j further validates this observation by showcasing the EDX spectrum and composition of PVC-MP adsorbed onto the pGel@IPN hydrogel.

The AFM analysis reveals a significant change in the surface roughness of the hydrogel. Initially, the RMS surface roughness (S_q) of the IPN hydrogel measures 22.32 nm, but after incorporating Cu-POM *in situ*, it notably increases to 93.29 nm, as depicted in Fig. 4(a and b). This enhanced roughness substantially contributes to the higher efficiency in capturing MPs by augmenting the surface area of the pGel@IPN hydrogel. Comparative analysis in Fig. 4(c and d) demonstrates the S_q values of 588.7 nm and 1226 nm for PVC and PP-MPs, respectively. Corroborating these findings, the BET surface

area assessment of the Cu-POM incorporated hydrogel showed an increased surface area of 35.11 m^2 g^{-1}. Further characterization through nitrogen adsorption and desorption isotherms (Fig. 4e) and pore size distribution curves (found in ESI Fig. S2†) reveals an average pore diameter of approximately 12.5 nm for pGel@IPN. The interparticle pore diffusion within the pGel@IPN hydrogel structure holds potential for effectively capturing smaller MPs. Through this mechanism, smaller MPs can diffuse into the porous structure of the hydrogel, allowing for their entrapment or adsorption within the triple IPN network. The intricate pore structure, likely facilitated by the increased surface roughness and expanded surface area due to the incorporation of Cu-POM, creates a conducive environment for MP capturing.

In conjunction with the surface roughness analysis, the evaluation of the hydrogel contact angle assesses its hydrophilicity, providing a comprehensive understanding of its surface

Fig. 4 AFM analysis to evaluate the RMS surface roughness (S_q) for (a) Gel@IPN, (b) pGel@IPN, (c) PVC-MPs, and (d) PP-MPs; (e) nitrogen adsorption–desorption isotherms for Gel@IPN, pGel@IPN and POM; and (f) comparison of water contact angles (WCAs) of hydrogels with varying material compositions (inset: an enlarged view of WCA).

Table 1 Different material compositions used to synthesize hydrogels and their respective nomenclature

Materials	Compositions (ratio)	Refer as
PVA : CS	1 : 2	Gel-1
PVA : CS	2.1	Gel-2
PVA : CS	1 : 1	Gel-3
PVA : CS : PANI	1 : 1 : 0.5	Gel@IPN
Cu-POM : PVA : CS : PANI	1 : 1 : 1 : 0.5	pGel@IPN

properties in the context of MP capturing efficiency. The contact angles, as depicted in Fig. 4f and detailed in Table 1 for various material ratios, consistently remain below 90 degrees. This signifies the hydrophilic nature of the hydrogel surfaces, enabling effective water adsorption. Increasing PVA content from a 1 : 2 to a 2 : 1 PVA : CS ratio (Fig. 4f) significantly enhances hydrophilicity, evidenced by reduced contact angle from 73.88 degrees (Gel-1) to 65.68 degrees (Gel-2). This is attributed to the hydrophilic properties of PVA, fostering stronger interactions between the polymer network and water molecules, resulting in a more stable bond within the PVA/CS network. Conversely, altering the equivalent ratio of CS and PVA yields minimal change in the contact angle. Furthermore, the addition of PANI increases the hydrophilicity to 52.28 degrees by establishing a triple interpenetrating polymer network for polyanilines. The structural heterogeneity of the IPN polymer plays a pivotal role in minimizing interfacial or surface free energy. Upon introducing Cu-POM nanoclusters, the contact angle experiences a further reduction to 50.24 degrees (as observed in Fig. 4f). This reduction stems from the significant presence of $-NH_2$ groups introduced by ethylene diamine ligands, supplementing the existing functional groups of polyanilines. This aligns with the Wenzel model, elucidating that increased roughness on hydrophilic surfaces enhances wettability, thereby reducing contact angles.

Structural and spectroscopic evidence. The analysis of the FTIR spectra of Gel@IPN, pGel@IPN, and MPs (PVC and PP) using a Spectrum FTIR provided insights into the molecular composition of these materials (Fig. 5a). Notably, the observed broad peak at 3255 cm^{-1} corresponds to –OH absorption, and peaks at approximately 1053 and 1422 cm^{-1} signify –C–O groups in PVA.[17,40] Within the CS/PVA composition, peaks at around 1460 cm^{-1} relate to –OH vibrations, and at 1712 cm^{-1}, characteristic peaks for carboxylic acid dimers were detected. The appearance of the 1580 cm^{-1} peak indicates the symmetric deformation of $-NH_3^+$ resulting from primary amino group ionization in an acidic medium, with the peak at 1410 cm^{-1} signifying the presence of a carboxylic acid in the polymers.[39] Additional characteristic absorption peaks at 1362 cm^{-1} and 1053 cm^{-1} further confirm the presence of chitosan, specifically the C–O stretching vibration and typical C–H stretching vibrations at 2910 cm^{-1}. A significant peak at ~1632 cm^{-1} suggests the formation of imine bonds (C–N), forming Schiff's base structures from the reaction between chitosan's amino groups and glutaraldehyde's aldehyde groups. Peaks ranging from 1100 to 1590 cm^{-1} represent PANI

characterization within the IPN hydrogel matrix, possibly overlapping with other hydrogel matrix material peaks. Moreover, the peaks around 915 cm^{-1} and 1039 cm^{-1} denote the presence of P_2Mo_5 polyoxoanions,[46,47] indicating the incorporation of Cu-POM within the hydrogel matrix. These distinct characterization peaks validate the successful formation of the triple-IPN hydrogel, pGel@IPN. Furthermore, pure PVC-MPs exhibit characteristic C–H stretching at around 2850–2949 cm^{-1} and C–Cl stretching at 834 cm^{-1},[48] while distinctive peaks at 834, 1317, and 1626 cm^{-1} characterize the PP-MPs.[2]

The XRD analysis aimed to assess the crystallinity of Gel@IPN, pGel@IPN, and MP particles, revealing distinct patterns (Fig. 5b). Notably, Gel@IPN and pGel@IPN hydrogel matrices exhibited a significant broad peak at around 20° (2θ) attributed to PVA's (101) plane, indicating a crystalline structure.[49] The presence of PANI may contribute to a peak at around 25° (2θ), although overlapping with the broader PVA peak.[27] Conversely, the XRD patterns for PVC-MPs displayed poor crystallinity, suggesting an amorphous structure.[50] In contrast, the XRD patterns of PP-MPs revealed sharp peaks with a bumpy baseline, indicative of both crystalline and amorphous regions in the material.[51] These findings provide valuable insights into the structural characteristics of the hydrogel matrix and MP particles, contributing to a comprehensive understanding of their material properties.

The XPS wide scan spectra of CS/PVA/PANI depicted in Fig. 5h reveals distinct peaks corresponding to C 1s (at 288 eV), O 1s (at 529.1 eV), and N 1s (at 400.6 eV), along with Cu 2p (at 935.2 eV) and Mo 3d (at 232 eV).[17,52,53] These findings unequivocally confirm the presence of all constituents within pGel@IPN, signifying the successful synthesis of the Cu-POM infused PVA/CS/PANI-based hydrogel. Deconvolution of the C 1s, N 1s, and Mo 3d peaks aimed to discern the oxidation states of these materials (Fig. 5(i–k)). The C 1s deconvolution revealed peaks attributed to C–C bonds at 284.32 eV, C–O at 285.57 eV, and C=O at 286.43 eV. Similarly, the deconvoluted N 1s peaks displayed distinct signals at 398.9 eV for C–N and 401.2 eV for NH_3^+. The Mo 2d deconvolution exhibited two oxidation states of Mo, one at around 231.8 eV (attributed to Mo $3d_{5/2}$) and the other at 334.64 eV (attributed to Mo $3d_{3/2}$). These observations collectively affirm the successful formation and composition of the pGel@IPN hydrogel, validating its structural integrity and constituent elements.

Thermal properties of the hydrogel. In this study, the thermal stability of Gel@IPN and pGel@IPN hydrogels, along with MP particles, was systematically investigated through thermogravimetric analysis (TGA), as depicted in Fig. 5g. The decomposition profiles revealed two distinct weight loss stages for the hydrogels within the temperature ranges of 50 °C–95 °C and 213–310 °C. The initial stage was attributed to moisture loss from the hydrogel compound, while the subsequent stage was linked to the degradation of polysaccharide chains in chitosan.[19,54] Interestingly, the TGA results showed no notable alteration in thermal stability when comparing the hydrogel formulations before and after the integration of Cu-POM nanoclusters. The result underscores the confirmed

Fig. 5 Comprehensive investigations of physiochemical characterization of hydrogels and MPs: (a) FTIR and (b) XRD patterns of the hydrogel and PVC and PP-MPs; (c) pGel@IPN hydrogel swelling comparisons with varied glutaraldehyde (GA) ratios; (d, e) images visually depicting the dry and water-swelled hydrogel, respectively; (f) mechanical stability assessment *via* tensile testing under different GA ratios, (inset: hydrogel shape for UTM analysis); (g) TGA plot for thermal behavior understanding; and (h) XPS survey spectra of the pGel@IPN hydrogel, and (i–k) deconvoluted XPS C 1s, N 1s, and Mo 3d peak of the pGel@IPN hydrogel.

stability of Cu-POM nanoclusters within the hydrogel matrix. The persistence of thermal stability despite the addition of Cu-POM nanoclusters suggests a synergistic relationship between the intrinsic stability of the hydrogel's IPN structure and the added stability contributed by the Cu-POM nanoclusters. This observation implies that the robustness of the triple network IPN structure played a pivotal role in conferring thermal stability to the hydrogel. Furthermore, the thermogravimetric curve of PVC-MPs exhibited no weight loss until 250 °C, indicating the absence of bound water. Subsequent stages, starting at 250 °C and 407.3 °C, involved significant weight losses (62.2 wt% and 23.34 wt%, respectively). The initial stage was associated with the breakage of C–Cl bonds, attributed to their

low bond dissociation energy, while the latter stage was indicative of the decomposition of oxygenated compounds and organic residues in PVC.[55] The research findings concluded comparatively lower thermal stability of plastic particles when compared with the IPN hydrogel, underscoring the pivotal role of the hydrogel's unique structure in maintaining thermal integrity.

Mechanical properties of the hydrogel under the tensile test. Fig. 5f illustrates the mechanical responses to uniaxial tension for pGel@IPN hydrogels, the base-blend (CS/PVA/PANI), and their crosslinked counterparts with varying concentrations of GA (1%, 2%, and 3% wt). The stress (MPa) *vs.* strain (%) curves depict non-linear behavior in the dried state, indicative of a

rubber-like characteristic. This suggests that the hydrogels, governed by the triple interpenetrating polymer networks (CA/PVA/PANI) with a fixed concentration (1 g) of POM composites, exhibit distinct mechanical responses. The pGel@IPN hydrogels demonstrated an average maximum strain (elongation at break) of 66.47%, while reaching a maximum stress of 4.1 MPa. This highlights the blend's enhanced elasticity in the absence of covalent crosslinking by GA. Conversely, upon GA crosslinking, a notable reduction in the maximum elongation at break was observed (57.3%, 44.8%, and 32.28% for GA concentrations of 1%, 3%, and 5% in the hydrogel, respectively). This effect is attributed to the modification of the network architecture by crosslinking reagents, introducing crosslinking points that restrict the movement and unfolding of polymer chains within the network.[56] Despite the decrease in elongation at break, the stress-carrying capacity is significantly enhanced through GA crosslinking. This approach is commonly employed to improve mechanical properties, and in this study, 1% GA is identified as optimal, striking a balance between moderate elongation at break and enhanced stress-carrying capacity. This consideration is crucial for the hydrogel's application in the removal of MPs from water.

Swelling of the hydrogel. Swelling experiments were conducted on POM-infused CS/PVA/PANI hydrogel samples (pGel@IPN), employing varied glutaraldehyde (GA) crosslinking proportions. Fig. 5c illustrates the characteristic swelling behavior before and after chemical crosslinking with 1%, 2%, and 5% GA content, spanning different time intervals. The observed pattern exhibited an initial rapid mass uptake within approximately 30 minutes, followed by stabilization over 12 hours, visually confirming a substantial volume increase (Fig. 5c and d). The expansion of the polymeric network occurs due to the hydrophilic nature of the hydroxyl and amino groups present in the chitosan backbone of the hydrogel, facilitating interaction with water molecules through hydrogen bonding.[57] The study revealed a pronounced influence of crosslinking on pGel@IPN hydrogel swelling, with the initial 626% swelling before crosslinking diminishing to 512%, 343%, and 298%, corresponding to 1%, 3%, and 5% v/v glutaraldehyde concentrations, respectively. This phenomenon is attributed to the formation of a more rigid network, particularly at higher GA concentrations, resulting from inter–intra polymer chain reactions. This rigidity reduced the flexibility and the number of hydrophilic groups, adversely affecting the swelling rate, in alignment with the hydrogel mechanism.[56] In the Pre-GA reaction, the PVA chains were physically entangled with chitosan chains, forming a hydrogel network. Subsequent increases in GA content induced chemical crosslinking, forming covalent bonds among chains (depicted in Fig. 5c), fixing and reducing polymer mobility, resulting in a lower swelling rate. However, crosslinking plays an important role in ensuring mechanical stability (see tensile test results) of hydrogels, notably for application in water remediation, including adsorbing MP contaminants from water. Crosslinking improves hydrogel characteristics by forming interpenetrated-interconnecting polymer networks between CS/PVA/PANI.

Therefore, a minimum 1% v/v GA crosslinking ratio was considered optimum for pGel@IPN formation, striking a balance between stability and effective MP pollutant adsorption in water environments.

3.2. Microplastic adsorption and reusability assessment of pGel@IPN from aqueous solutions

In this research, batch adsorption investigations were conducted to explore the removal of MPs from contaminated water using the pGel@IPN hydrogel. The experiments involved varying parameters, such as pH, MP concentration, hydrogel dosage, contact time, and temperature, to simulate real-world scenarios and optimize the adsorption process. Fig. 6(a and b) illustrates the dispersion of the pGel@IPN hydrogel in MP contaminated water, followed by visual confirmation of MPs adhering to the spent hydrogel post-adsorption. Furthermore, SEM analysis (Fig. 6c) confirmed the embedding of PVC-MPs within the mixed matrix IPN hydrogel. Besides, fluorescence-stained MP images captured *via* fluorescence confocal microscopy (Fig. 6d and e) corroborated successful PVC and PP-MP adsorption onto the hydrogel. These images depicted fluorescent-tagged MP particles both adhering to the hydrogel's surface and embedded within its matrix, supporting effective MP adsorption. The porous structure (pore dia. 12.5 nm) and polymeric entanglements of the triple IPN hydrogel significantly facilitated MP capture. Additionally, the presence of functional groups, particularly amino groups from chitosan and PANI in the IPN hydrogel, attracted and facilitated the adsorption of negatively charged MPs.

However, the pH of the media plays a very crucial role in the adsorption phenomenon of MPs by the pGel@IPN hydrogel. In Fig. 6f, we explored the MP removal efficiency across different initial solution pH levels. The results highlighted a substantial impact of the initial pH on the hydrogel's MP removal performance.[58] Notably, the hydrogel exhibited high MP removal efficiency, ranging from 78.8% to 95.5% for PVC and 83.5% to 93.3% for PP particles within a solution pH range of 2.5 to 6.5. However, with the solution pH greater than 7 and approaching 12, a decrease in MP removal efficiency was observed. This observed variation in efficiency can be attributed to electrostatic interactions between MPs and the pGel@IPN hydrogel. The point of zero charge (PZC) obtained from the zeta potential analysis of MP particle and hydrogels elucidated this process. Fig. 6g illustrates the PZC for the pGel@IPN hydrogel, approximately at pH 6.4. In contrast, PVC and PP-MPs exhibited PZCs at pH 2.5 and pH 2.9, respectively. Particularly, below the PZC (pH < PZC), the surface charge of the materials is positive, while above the PZC (pH > PZC), it is negative. Within the pH range of 2.5 to 6.5, both the MPs and pGel@IPN hydrogel possessed opposite charges, resulting in strong electrostatic attraction.[59] This mechanism facilitated the effective removal of MP particles from contaminated water within a neutral pH range, prompting further experiments under these conditions. However, once the solution pH exceeded the PZC, electrostatic repulsion began to hinder the interaction between the pGel@IPN hydrogel and MPs, result-
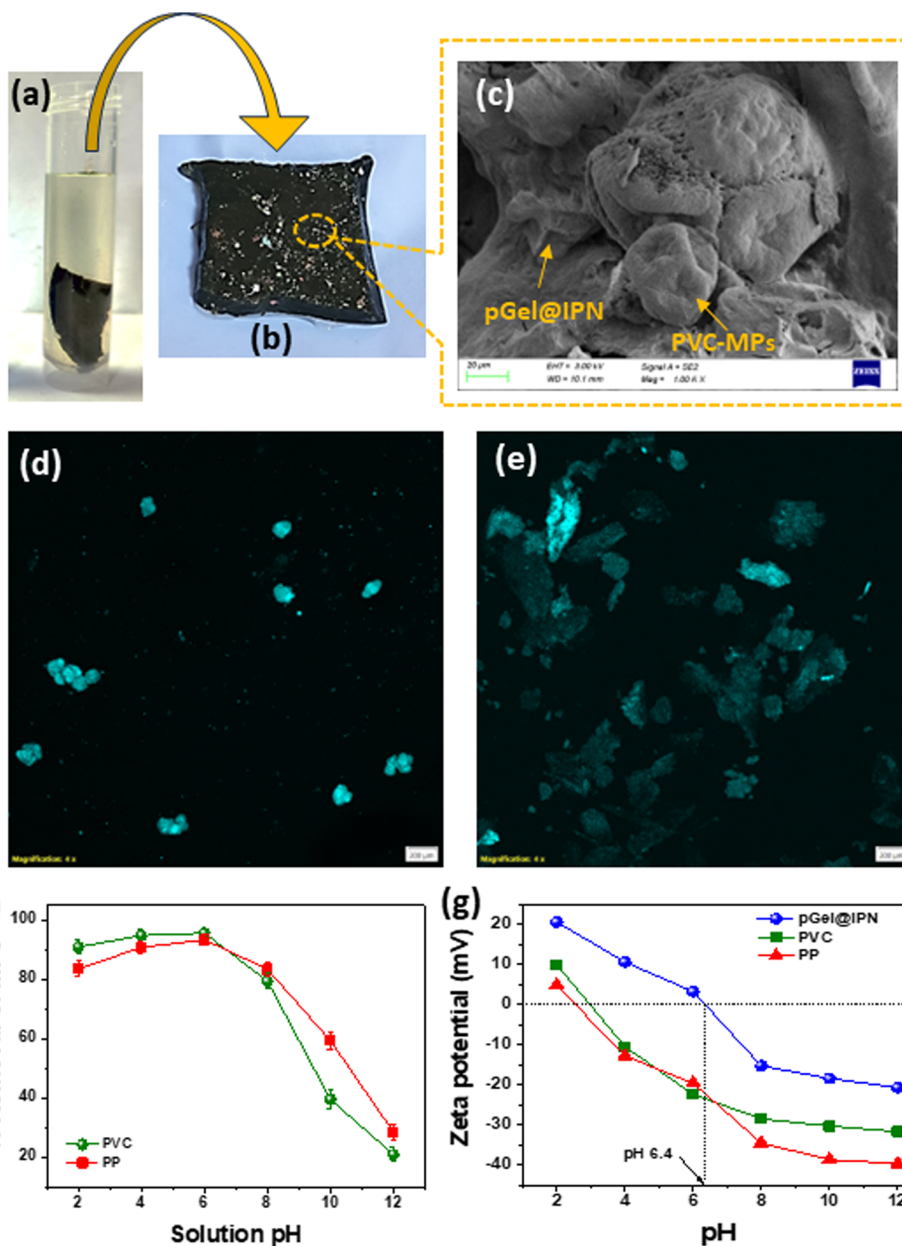
Fig. 6 Illustrates (a) the treatment of MP contaminated water using the pGel@IPN hydrogel; (b) images displaying MP-adsorbed hydrogel post-removal; (c) SEM images demonstrating the PVC-MPs adsorbed pGel@IPN hydrogel matrix; (d–e) fluorescence confocal microscopy images of Nile red-labeled PVC-MPs and PP-MPs adsorbed hydrogel, respectively; (f) MP removal efficiency at different water pH levels; and (g) zeta potential analysis to determine the PZC of hydrogel and MP particles across varying solution pH levels.

ing in a gradual decrease in MP removal efficiency. The study highlights the significance of pH-dependent electrostatic interactions in MP removal. Besides pH, the adsorption of MPs is facilitated by the structural and surface features of hydrogels, enhancing the capture of MPs in aquatic environments through improved polymer network entanglement in IPN hydrogels.

Additionally, the optimum adsorbent (hydrogel) dosage and its influence on removal efficiency of PVC-and PP-MPs are investigated, as shown in Fig. S3a (ESI†). At an optimal solution pH of ~6.5, increasing the dosage of the pGel@IPN hydro-

gel led to a notable augmentation in MP removal efficiency, reaching around 96% for PVC and 94% for PP-MPs. This increased efficacy is attributed to the enhanced active surface area provided by higher doses of the adsorbent, facilitating improved MP adsorption.[25,27] The study found that beyond 1 g L^{-1} pGel@IPN hydrogel, there was no notable increase in MP removal efficiency, indicating it as the optimum adsorption dose. Furthermore, a higher initial MP concentration reduced the adsorption efficiency at a constant hydrogel dose, suggesting active site saturation at higher concentrations, as shown in Fig. S3b.† Furthermore, the study illustrates the sus-

tainable reusability of the IPN hydrogel for efficient removal of PVC and PP-MPs. After drying and reintroduction into MP contaminated water for up to 5 cycles (~65.4% removal, Fig. 8d), the hydrogel maintains efficacy. However, effectiveness gradually decreases after 5 cycles, indicating hydrogel exhaustion with MPs. This reusability could be attributed to the hydrogel's highly active adsorption sites and the entanglement of polymeric networks within the IPNs, facilitating the effective capture of MP particles.

3.3. Microplastic adsorption kinetics and isotherm study

The investigation into the adsorption kinetics of MP particles onto the hydrogel is pivotal for comprehending the rate of the adsorption process. Kinetic analyses offer crucial insights into the temporal relationship and mass transfer phenomena of the adsorbent in the adsorption process, shedding light on underlying mechanisms such as chemical reactions and diffusion. The MP removal efficiency at various contact times is shown in Fig. S3c.† The results show that both the PVC and PP-MP removal achieve equilibrium with >94% removal efficiency at around 290 min. Initially, the adsorption occurs rapidly followed by gradually reaching saturation. In this study, pseudo-first-order, pseudo-second-order, and interparticle penetration kinetics (refer Fig. 7a–c), were applied by fitting these models to the time variation data. The fitting results are tabulated in ESI Table S1.† The data indicated that the pseudo-second-order kinetics model exhibited an excellent fit for both PVC ($R^2 = 0.99$) and PP ($R^2 = 0.98$) MP adsorption. The suitability of the pseudo-second-order kinetic model suggests that chemisorption likely plays a significant role in the adsorption process.[27] Additionally, the Weber–Morris intraparticle diffusion model was employed to determine the rate-controlling mechanism of MP adsorption onto the pGel@IPN hydrogel, utilizing the q_t vs. $t^{0.5}$ plot as displayed in Fig. 7c. The results, presented in Table S2 (ESI†), revealed a three-stage regression fit that did not intersect the origin of the plot for both MP types. The initial steep phase indicated rapid extraction of MPs from the water medium, governed by surface or film diffusion, potentially attributed to the highly available active sites within the pGel@IPN hydrogel matrix. Subsequently, a gradual adsorption process was observed, driven by intraparticle or pore diffusion. The final phase suggested equilibrium attainment.[25,60] This comprehensive study underscores that the adsorption of PVC and PP-MPs onto the hydrogel is influenced not only by intraparticle diffusion (pore diffusion) but also by film diffusion (external mass transfer), providing valuable insights for the design of efficient MP removal strategies.

Examining the adsorption equilibrium between the adsorbent and adsorbate interface until reaching equilibrium is crucial and is described through adsorption isotherm studies (Fig. 7d and e). Experimental data were fitted to two theoretical isotherm models—Langmuir and Freundlich—as detailed in the Experimental section, to elucidate the adsorption process of MPs onto the hydrogel matrix. The fitting results are tabulated in ESI Table S2.† Statistical analysis reveals that the adsorption of both PVC and PP-MPs adheres to the Langmuir model, evident from the correlation coefficient (R^2) values greater than 0.99. The excellent fitting of the Langmuir isotherm model suggests that the adsorption of both MPs by the

Fig. 7 Kinetic data fitted in (a–b) pseudo-second-order kinetic models for the adsorption of PVC and PP-MPs, respectively, (c) the Weber–Morris intraparticle diffusion model for the adsorption PVC and PP-MPs onto the pGel@IPN hydrogel. Experimental data fitted to Langmuir and Freundlich isotherm models for (d) PVC and (e) PP-MPs adsorption onto the pGel@IPN hydrogel. (f) Van't Hoff plots for MPs adsorption onto the pGel@IPN hydrogel matrix, providing insights into the thermodynamic parameters. (Experimental conditions: temperature: 25 ± 3 °C, initial MPs concentration: 25 mg L^{-1}, pGel@IPN hydrogel dose: 1 g L^{-1}, pH: ~6.5.)

pGel@IPN hydrogel primarily occurs homogeneously on the surface *via* monolayer sorption.[27] The calculated Q_m values, representing the maximum adsorption capacity, are notably high, reaching 321.87 mg g^{-1} for PVC and 144.29 mg g^{-1} for PP-MP adsorption onto the hydrogel. These findings underscore the applicability of the Langmuir isotherm model in describing the adsorption behavior of PVC and PP-MPs onto the hydrogel. The high Q_m values indicate a substantial capacity of the hydrogel to adsorb and remove these MPs, supporting its potential as an effective adsorbent for environmental remediation.

3.4. Thermodynamic study

The adsorption characteristics of PVC and PP-MPs onto the hydrogel were explored across varying temperatures (293 K, 303 K, and 313 K) through a thermodynamic investigation. Thermodynamic parameters such as the change in Gibb's free energy ($\Delta G°$), entropy ($\Delta S°$), and enthalpy ($\Delta H°$) were determined using eqn (9)–(11):[27]

$$\Delta G° = RT \ln K_C \qquad (9)$$

$$\ln K_C = \frac{-\Delta H°}{RT} + \frac{\Delta S°}{R} \qquad (10)$$

$$\Delta G° = \Delta H° - T\Delta S° \qquad (11)$$

The parameters R (universal gas constant, 8.314 J mol^{-1} K^{-1}) and T (temperature in Kelvin) are utilized, along with the equilibrium constant, $K_C = q_e/C_e$, to obtain insights into the energetic and spontaneous nature of the adsorption process. The values of $\Delta H°$ (kJ mol^{-1}) and $\Delta S°$ (kJ mol^{-1} K^{-1}) were determined from the slope and intercept of the Van't Hoff plot, $\ln K_C$ *versus* $1/T$, illustrated in Fig. 7f (Table S3†). The negative $\Delta G°$ values, decreasing with rising temperature, affirm the feasibility and spontaneity of PVC and PP microplastics' adsorption onto the pGel@IPN hydrogel. Positive $\Delta H°$ and $\Delta S°$ values indicate an endothermic process and increased randomness at the adsorbent/adsorbate interface. As temperature increases, the larger pore size within the interpenetrating polymer network of the hydrogel facilitates deeper penetration of MPs, contributing to enhanced removal efficiency. This temperature-dependent behavior underscores the thermodynamic characteristics governing the effective adsorption of MPs onto the hydrogel.

3.5. Photocatalytic degradation of microplastics by pGel@IPN

The study explores the application of photocatalytic degradation to tackle MP pollution, specifically focusing on PVC-MP particles adsorbed onto a hydrogel through photocatalysis in an aqueous environment. In this investigation, the photodegradation process is facilitated by Cu-POM present in the pGel@IPN matrix. POMs are utilized as photocatalysts due to several advantageous properties: their redox capability, adaptable stability, distinct active sites within their crystal structures, and tunable light absorption through the introduction of transition metals into the POMs.[8,33,61,62] However, to evaluate the photocatalytic properties, the band gap energy of Cu-POM was determined using the Tauc plot, as detailed in ESI, S2.† Fig. S5a† depicts the UV–vis spectra of Cu-POM nanoclusters in water, revealing an adsorption band extending into the UV region. This characteristic contributes to the nanocomposite's exceptional photocatalytic performance in the UV range. Fig. S5b† describes the calculation of the corresponding band gap energy value for Cu-POM, resulting in a value of 2.87 eV, this aligns closely with the reported band gap value (2.9 eV) for another Keggin-type POM in the literature.[63] During UV irradiation in the photodegradation test, energy equivalent to or greater than the band gap drives electron excitation, resulting in the production of reactive oxygen species (ROS), such as hydroxyl radicals (˙OH) and superoxide radicals (O$_2$˙$^-$), which are essential for MP breakdown.

The photocatalytic degradation mechanism involves breaking down of MP polymer chains into smaller fragments, generating intermediates and byproducts like CO_2 and H_2O. POMs act as effective scavengers, capturing photogenerated electrons and converting them into reduced POM species. These species transfer electrons to dissolved oxygen, forming oxygen radicals (O$_2$˙$^-$). The radicals interact with water, generating ˙OH species and enhancing MP oxidation, accelerated by the POM-infused IPN hydrogel (pGel@IPN), as shown in Fig. 8a. However, the progression of degradation was monitored *via* morphological changes through SEM images (Fig. 8b and c). Initial observations (Fig. 8b) indicated a 100 μm average diameter for commercial PVC-MPs. After 10 hours of UV exposure for photocatalytic degradation, the average diameter decreased to approximately 55 μm (Fig. 8c). PVC microparticle photodegradation was quantified using eqn (12), assessing the degradation efficiency based on the size change.

$$\text{Microplastics degradation efficiency}\% = \frac{D_0 - D_t}{D_0} \times 100\% \quad (12)$$

Here, D_0 represents the initial average diameter of MPs, and D_t represents the average diameter after a specified photodegradation time 't'. The findings reveal a degradation efficiency of approximately 45% for PVC-MPs exposed to UV radiation in concurrence with a POM-infused hydrogel. The SEM images (Fig. 8b, marked by a white circle) provide visual evidence supporting the notion that PVC-MPs undergo degradation, disintegrating into smaller particles, although complete degradation has not been achieved.[64]

Moreover, the photodegradation of MPs may lead to the formation of intermediate products. The potential intermediates in the degradation pathways of MPs may include various substances such as alkenes, ketones, alcohols, aldehydes, lactones, ketoacids, and esters.[65] Previous studies propose a degradation pathway for PVC-MPs involving sequential steps.[65] Initially, PVC-MPs attack the C–Cl bond, initiating dichlorination under UV light.[66] Then, dehydrochlorination occurs, producing carbo-cations transformed into alkene and polyene (C=C) structures.[65,67,68] In subsequent steps, PVC-MPs could be oxidized by O_2 and H_2O, forming oxygen-containing
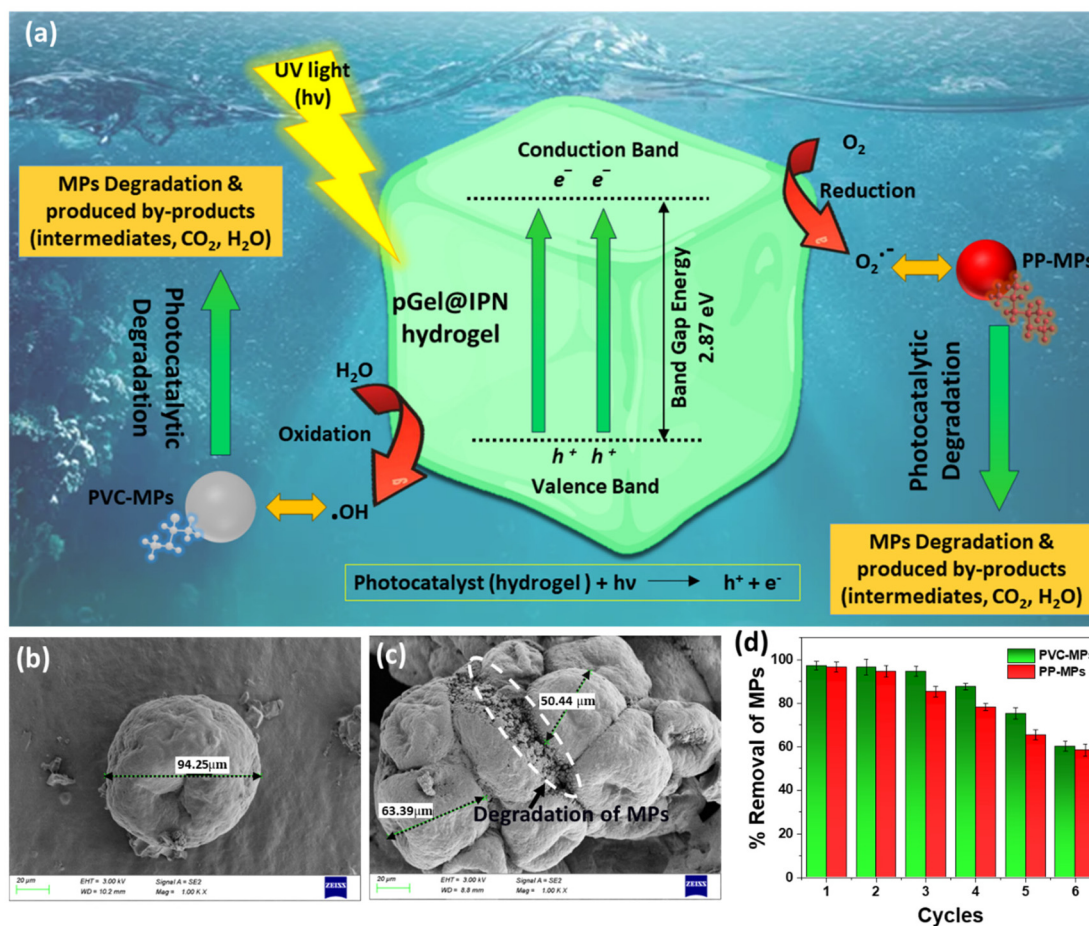
Fig. 8 (a) Schematic representation of the photocatalytic degradation process of MP particles; (b) SEM images of commercial PVC–MP particle; (c) after photocatalytic degradation the deformed PVC–MPs; and (d) reusability of pGel@IPN hydrogel for MPs removal efficiency.

groups (*e.g.*, alcohols, ketones) in the water solution.[65,69] Furthermore, hydrocarbon-based substances undergo attack by $O_2^{\bullet-}$ radicals, forming smaller substances like alcohols, carboxylic acids, and esters, eventually degrading into CO_2 and H_2O. Nevertheless, in our instance, the potential for generating similar intermediates during the breakdown of PVC-MPs in the presence of Cu-POM cannot be ruled out. however, achieving complete MP breakdown into CO_2 and H_2O in our experimental setup remains challenging.

3.6. Enabling circular economy: upcycling the spent hydrogel to carbon nanomaterials for sustainable heavy metal removal

Upon reaching saturation and the end of life (EoL), the spent pGel@IPN hydrogel matrix becomes saturated with PVC and PP-MPs. Direct disposal of this exhausted material poses environmental risks, potentially re-contaminating the environment with MP particles. Post-adsorption, sustainable management of spent adsorbent becomes imperative. Instead of single-use disposal, regenerating, recycling, or repurposing the material aligns with circular economy principles, minimizing waste and optimizing resource utilization. In this context, we

implemented an upcycling strategy by transforming the spent MPs-exhausted hydrogel into highly effective carbon nanomaterials, specifically named carbon dots (CDs). The synthesis process involved a two-step procedure comprising thermal calcination and subsequent hydrothermal treatment. The spent adsorbents were uniformly heated to 300 °C for 2 hours, with a temperature ramp rate of 10 °C min^{-1}, followed by further elevation to 700 °C for an additional 1 hour. Subsequently, a hydrothermal treatment was conducted at 200 °C for 5 hours using deionized water.[70,71] SEM analysis confirmed the formation of carbon nanomaterials, revealing nano-spherical particles with an average size of approximately 550 nm (Fig. 9, top of the triangle). These carbon nanoparticles, rich in surface functional groups, were utilized as an adsorbent for the removal of toxic hexavalent chromium (Cr(VI)) from contaminated water. The results showcased exceptional adsorption behavior, underscoring the efficacy of the upcycled carbon nanomaterials for environmental remediation (Fig. 9).

This upcycling strategy not only addresses environmental concerns related to spent adsorbents but also demonstrates the potential of these transformed materials in environmental
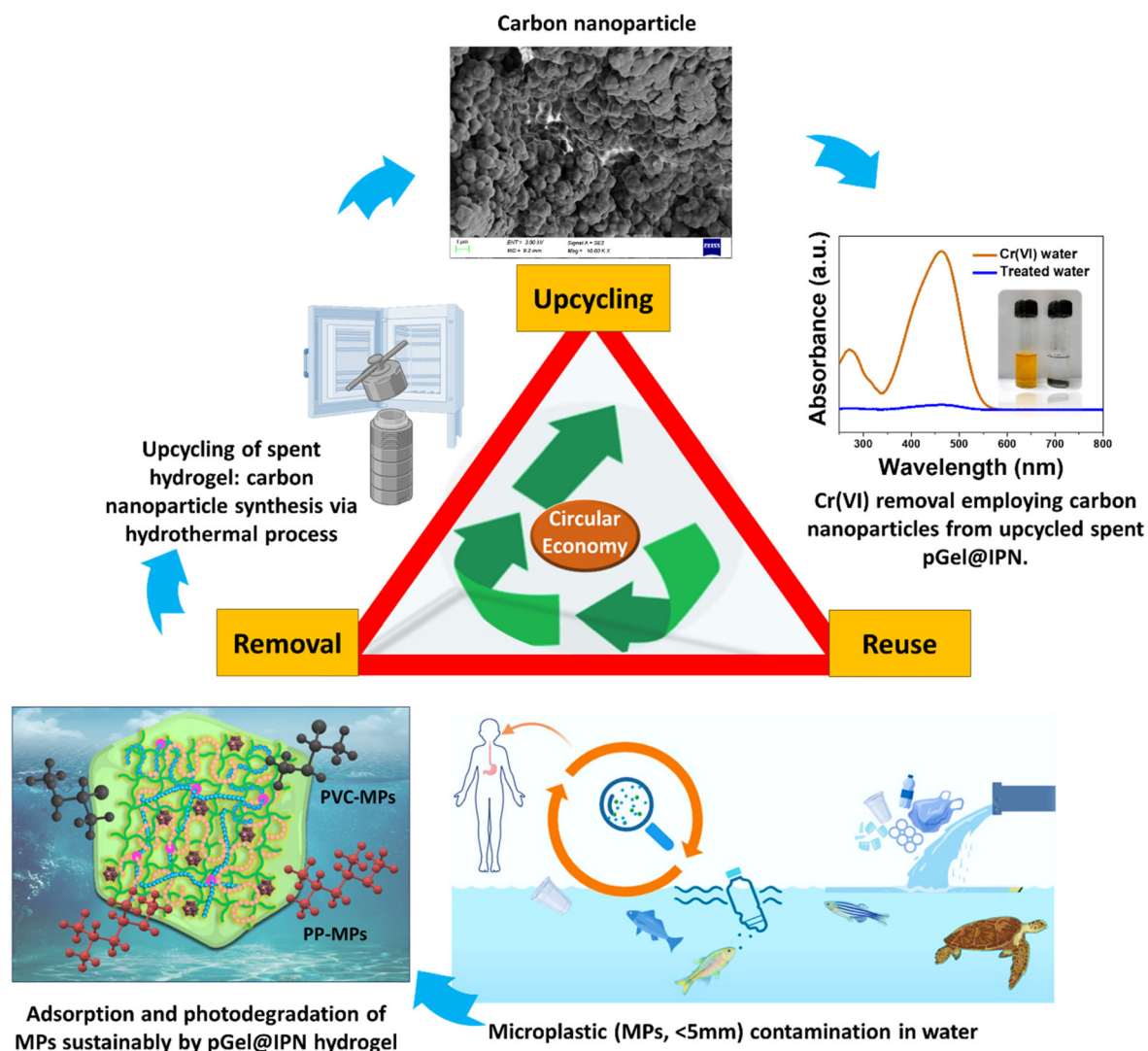
Fig. 9 Depicts the comprehensive lifecycle of the pGel@IPN hydrogel material, demonstrating its transformation from a MP adsorbent into upcycled valuable carbon nanomaterials, promoting circular economy principles, and emphasizing its role in sustainable practices and its potential for managing toxic heavy metals.

remediation. The schematic representation in Fig. 9 illustrates the comprehensive lifecycle of the prepared pGel@IPN hydrogel material, showcasing its transformation from an excellent microplastic adsorbent to its post-EoL upcycling into carbon nanomaterials for efficient Cr(vi) adsorption. This emphasizes the viability of a sustainable and eco-friendly material management strategy.

4. Conclusion

In conclusion, this study introduces a sustainable solution for tackling microplastic (MP) contamination in water, utilizing a Cu-POM-infused triple IPN hydrogel, termed pGel@IPN, composed of chitosan, PVA, and PANI. Through comprehensive investigations under diverse experimental conditions resem-

bling real-world scenarios, we elucidated the detailed adsorption behaviors of model MPs (PVC and PP) onto the hydrogel matrix. The physicochemical properties, mechanical strength, and thermal behavior analyses highlighted the robustness and stability of the synthesized hydrogel. Initial labeling of MPs with Nile red facilitated their detection and analysis *via* fluorescence microscopy. The pGel@IPN hydrogel demonstrated exceptional MP removal efficiency, reaching approximately 95% for PVC and 93% for PP-MPs at neutral pH (~6.5). Additionally, the catalytic properties of POM within the hydrogel facilitated the degradation of adsorbed MPs under UV irradiation, presenting a sustainable approach to mitigate MP contamination in water. The dual functionality of capturing and degrading MPs positions the pGel@IPN hydrogel as an environmentally friendly strategy. Detailed kinetics and isotherm studies highlighted the efficacy of the pseudo-first-order

and Langmuir isotherm models, emphasizing high maximum adsorption capacity (Q_m). Moreover, the pGel@IPN hydrogel exhibited reusability, sustaining up to 5 cycles of MP removal. Beyond its primary function, the spent adsorbent was successfully upcycled into carbon nanomaterials, serving as an effective adsorbent for removing the heavy metal Cr(VI) from contaminated water, aligning with circular economy principles. Overall, our prepared hydrogel emerges as a promising and effective solution for addressing MP pollution in water in a sustainable manner.

Author contributions

SD: conceptualization, experimentation, original draft writing, reviewing and editing; SB: conceptualization, providing resources, supervision, and review; AM: constructive inputs and feedback.

Conflicts of interest

The authors have no conflicts to declare.

Acknowledgements

References

1 A. A. Koelmans, N. H. Mohamed Nor, E. Hermsen, M. Kooi, S. M. Mintenig and J. De France, *Water Res.*, 2019, **155**, 410–422.

2 H. Luo, C. Liu, D. He, J. Sun, A. Zhang, J. Li and X. Pan, *Water Res.*, 2022, **222**, 118921.

3 S. Liu, E. Shang, J. Liu, Y. Wang, N. Bolan, M. B. Kirkham and Y. Li, *Front. Environ. Sci. Eng.*, 2022, **16**, 8.

4 N. Bostan, N. Ilyas, N. Akhtar, S. Mehmood, R. U. Saman, R. Z. Sayyed, A. A. Shatid, M. Y. Alfaifi, S. E. I. Elbehairi and S. Pandiaraj, *Environ. Res.*, 2023, **234**, 116523.

5 Md. N. Rahman, S. H. Shozib, M. Y. Akter, A. R. Md. T. Islam, Md. S. Islam, Md. S. Sohel, C. Kamaraj, Md. R. J. Rakib, A. M. Idris, A. Sarker and G. Malafaia, *J. Hazard. Mater.*, 2023, **454**, 131522.

6 K. Kim, J. Min, M. Lee, G. Sim, S. S. Oh and M. J. Park, *Nanoscale*, 2022, **14**, 17157–17162.

7 Q. Guo, Y. Liu, J. Liu, Y. Wang, Q. Cui, P. Song, X. Zhang and C. Zhang, *Chem. Mater.*, 2022, **34**, 5165–5175.

8 A. Misra, C. Zambrzycki, G. Kloker, A. Kotyrba, M. H. Anjass, I. Franco Castillo, S. G. Mitchell, R. Güttel and C. Streb, *Angew. Chem., Int. Ed.*, 2020, **59**, 1601–1605.

9 P. Chattopadhyay, M. C. Ariza-Tarazona, E. I. Cedillo-González, C. Siligardi and J. Simmchen, *Nanoscale*, 2023, **15**, 14774–14781.

10 Y. Guo, J. Bae, Z. Fang, P. Li, F. Zhao and G. Yu, *Chem. Rev.*, 2020, **120**, 7642–7707.

11 V. Van Tran, D. Park and Y.-C. Lee, *Environ. Sci. Pollut. Res.*, 2018, **25**, 24569–24599.

12 S. Dutta, R. Sen Gupta, S. Pathan and S. Bose, *RSC Adv.*, 2023, **13**, 6087–6107.

13 S. Dutta, R. Sen Gupta, K. Manna, S. Safikul Islam and S. Bose, *Chem. Eng. J.*, 2023, **472**, 145008.

14 Z. Zhang, Q. Dou, S. Wang, D. Hu, B. Yang, Z. Zhao, H. Liu and Q. Dai, *Nanoscale*, 2020, **12**, 22787–22797.

15 S. Ganguly, P. Das, P. P. Maity, S. Mondal, S. Ghosh, S. Dhara and N. Ch. Das, *J. Phys. Chem. B*, 2018, **122**, 7201–7218.

16 C. Cheng, Z. Liu, X. Li, B. Su, T. Zhou and C. Zhao, *RSC Adv.*, 2014, **4**, 42346–42357.

17 R. Liu, X. Xu, X. Zhuang and B. Cheng, *Carbohydr. Polym.*, 2014, **101**, 1116–1121.

18 L. Jin and R. Bai, *Langmuir*, 2002, **18**, 9765–9770.

19 D. R. Barleany, Jayanudin, A. S. Utama, U. Riyupi, H. Alwan, R. S. D. Lestari, A. B. Pitaloka, M. Yulvianti and Erizal, *Mater. Today: Proc.*, 2023, **87**, 1–7.

20 Y. Chen, C. Jiao, X. Peng, T. Liu, Y. Shi, M. Liang and H. Wang, *J. Mater. Chem. B*, 2019, **7**, 3243–3249.

21 F. Ahmadijokani, H. Molavi, A. Bahi, S. Wuttke, M. Kamkar, O. J. Rojas, F. Ko and M. Arjmand, *Chem. Eng. J.*, 2023, **457**, 141176.

22 S. Panpinit, S. Pongsomboon, T. Keawin and S. Saengsuwan, *React. Funct. Polym.*, 2020, **156**, 104739.

23 J. Fu, F. Yang and Z. Guo, *New J. Chem.*, 2018, **42**, 17162–17180.

24 C. Ulutürk and N. Alemdar, *Carbohydr. Polym.*, 2018, **193**, 307–315.

25 S. Dutta, S. K. Srivastava and A. K. Gupta, *Mater. Adv.*, 2021, **2**, 2431–2443.

26 S. Dutta, K. Manna, S. K. Srivastava, A. K. Gupta and M. K. Yadav, *Sci. Rep.*, 2020, **10**, 4982.

27 S. Dutta, S. K. Srivastava, B. Gupta and A. K. Gupta, *ACS Appl. Mater. Interfaces*, 2021, **13**, 54324–54338.

28 J. Arichi, M. M. Pereira, P. M. Esteves and B. Louis, *Solid State Sci.*, 2010, **12**, 1866–1869.

29 J. Lu, Y. Xu, N. K. Goh and L. S. Chia, *Chem. Commun.*, 1998, 2733–2734.

30 D. Li, P. Ma, J. Niu and J. Wang, *Coord. Chem. Rev.*, 2019, **392**, 49–80.

31 A. Malakar, S. Mandal, R. Sen Gupta, S. S. Islam, K. Manna and S. Bose, *Nanoscale*, 2023, **15**, 3805–3822.

32 J. Lan, Y. Wang, B. Huang, Z. Xiao and P. Wu, *Nanoscale Adv.*, 2021, **3**, 4646–4658.

33 M. Aureliano, *BioChem*, 2022, **2**, 8–26.

34 S. Dutta, B. G. M. Patel, Y. Singh, G. Hegde and S. Bose, *J. Membr. Sci.*, 2024, 122422.

35 K. Enoch, C. S. Rakavi and A. A. Somasundaram, *Surf. Interfaces*, 2023, **41**, 103178.

36 S. Sharma, R. Kumar, N. Kumar Rana and B. Koch, *Eur. Polym. J.*, 2022, **180**, 111605.

37 Y. Ou and M. Tian, *J. Mater. Chem. B*, 2021, **9**, 7955–7971.

38 E. A. Kamoun, X. Chen, M. S. Mohy Eldin and E.-R. S. Kenawy, *Arabian J. Chem.*, 2015, **8**, 1–14.

39 T. Wang, M. Turhan and S. Gunasekaran, *Polym. Int.*, 2004, **53**, 911–918.

40 J. M. Yang, W. Y. Su, T. L. Leu and M. C. Yang, *J. Membr. Sci.*, 2004, **236**, 39–51.

41 H. Xie, Q. Yu, J. Mao, S. Wang, Y. Hu and Z. Guo, *J. Mater. Sci.: Mater. Electron.*, 2020, **31**, 10381–10389.

42 Y. Lan, E. Wang, Y. Song, Y. Song, Z. Kang, L. Xu and Z. Li, *Polymer*, 2006, **47**, 1480–1485.

43 P. J. Kulesza, M. Chojak, K. Karnicka, K. Miecznikowski, B. Palys, A. Lewera and A. Wieckowski, *Chem. Mater.*, 2004, **16**, 4128–4134.

44 W. Qi and L. Wu, *Polym. Int.*, 2009, **58**, 1217–1225.

45 S. J. Kim, S. J. Park and S. I. Kim, *React. Funct. Polym.*, 2003, **55**, 53–59.

46 C. Xing, J. Chang, M. Ma, P. Ma, L. Sun and M. Li, *J. Colloid Interface Sci.*, 2022, **612**, 664–678.

47 J. Shi, C. Wang, K. Yu, Z. Su, C. Wang and B. Zhou, *J. Coord. Chem.*, 2014, **67**, 2229–2237.

48 S. Ramesh, K. H. Leen, K. Kumutha and A. K. Arof, *Spectrochim. Acta, Part A*, 2007, **66**, 1237–1242.

49 P. B. Palani, K. S. Abidin, R. Kannan, M. Sivakumar, F.-M. Wang, S. Rajashabala and G. Velraj, *RSC Adv.*, 2014, **4**, 61781–61789.

50 Z.-Z. Bao, Z.-F. Chen, S.-Q. Lu, G. Wang, Z. Qi and Z. Cai, *Sci. Total Environ.*, 2021, **790**, 148077.

51 D. S. Moura, C. J. Pestana, C. F. Moffat, J. Hui, J. T. S. Irvine and L. A. Lawton, *Chemosphere*, 2023, **331**, 138691.

52 D. Lachowicz, A. Kmita, R. Wirecka, K. Berent, M. Szuwarzyński, S. Zapotoczny, A. Pajdak, G. Cios, N. Mazur-Panasiuk, K. Pyrc and A. Bernasik, *Carbohydr. Polym.*, 2023, **312**, 120756.

53 C. Luo, A. Guo, Y. Zhao and X. Sun, *Carbohydr. Polym.*, 2022, **286**, 119268.

54 P. Sharma, M. Sharma, H. Laddha, M. Agarwal and R. Gupta, *ACS Agric. Sci. Technol.*, 2023, **3**, 1068–1080.

55 W. Li, Z. Bai, T. Zhang, Y. Jia, Y. Hou, J. Chen, Z. Guo, L. Kong, J. Bai and W. Li, *Fuel*, 2023, **340**, 127555.

56 E. S. Costa-Júnior, E. F. Barbosa-Stancioli, A. A. P. Mansur, W. L. Vasconcelos and H. S. Mansur, *Carbohydr. Polym.*, 2009, **76**, 472–481.

57 I. M. Garnica-Palafox and F. M. Sánchez-Arévalo, *Carbohydr. Polym.*, 2016, **151**, 1073–1081.

58 S. Gunasekaran, T. Wang and C. Chai, *J. Appl. Polym. Sci.*, 2006, **102**, 4665–4671.

59 R. Yan, S. Lin, W. Jiang, X. Yu, L. Zhang, W. Zhao and Q. Sui, *Sci. Total Environ.*, 2023, **898**, 165431.

60 P. K. Mishra, R. Kumar and P. K. Rai, *Nanoscale*, 2018, **10**, 7257–7269.

61 J. Gu, W. Chen, G.-G. Shan, G. Li, C. Sun, X.-L. Wang and Z. Su, *Mater. Today Energy*, 2021, **21**, 100760.

62 O. M. Primera-Pedrozo, S. Tan, D. Zhang, B. T. O'Callahan, W. Cao, E. T. Baxter, X.-B. Wang, P. Z. El-Khoury, V. Prabhakaran, V.-A. Glezakou and G. E. Johnson, *Nanoscale*, 2023, **15**, 5786–5797.

63 S. Sampurnam, S. Muthamizh, T. Dhanasekaran, D. Latha, A. Padmanaban, P. Selvam, S. A. Stephen and N. V. Narayananan, *J. Photochem. Photobiol., A*, 2019, **370**, 26–40.

64 M. C. Ariza-Tarazona, J. F. Villarreal-Chiu, J. M. Hernández-López, J. Rivera De La Rosa, V. Barbieri, C. Siligardi and E. I. Cedillo-González, *J. Hazard. Mater.*, 2020, **395**, 122632.

65 L. Ding, X. Yu, X. Guo, Y. Zhang, Z. Ouyang, P. Liu, C. Zhang, T. Wang, H. Jia and L. Zhu, *Water Res.*, 2022, **208**, 117879.

66 F. Miao, Y. Liu, M. Gao, X. Yu, P. Xiao, M. Wang, S. Wang and X. Wang, *J. Hazard. Mater.*, 2020, **399**, 123023.

67 J.-L. Gardette and J. Lemaire, *Polym. Degrad. Stab.*, 1991, **34**, 135–167.

68 L. Jian, Z. Dafei and Z. Deren, *Polym. Degrad. Stab.*, 1991, **31**, 1–7.

69 C. Wang, Z. Xian, X. Jin, S. Liang, Z. Chen, B. Pan, B. Wu, Y. S. Ok and C. Gu, *Water Res.*, 2020, **183**, 116082.

70 M. Kumari and S. Chaudhary, *Colloids Surf., B*, 2020, **196**, 111333.

71 Y. Guo, Y. Feng, H. Li, Y. Wang, Z. Wen and G. Zhou, *Carbon*, 2022, **189**, 142–151.